



# CHORUS

This is the accepted manuscript made available via CHORUS. The article has been published as:

## Unconventional Chiral Fermions and Large Topological Fermi Arcs in RhSi

Guoqing Chang, Su-Yang Xu, Benjamin J. Wieder, Daniel S. Sanchez, Shin-Ming Huang, Ilya Belopolski, Tay-Rong Chang, Songtian Zhang, Arun Bansil, Hsin Lin, and M. Zahid Hasan

Phys. Rev. Lett. **119**, 206401 — Published 17 November 2017

DOI: [10.1103/PhysRevLett.119.206401](https://doi.org/10.1103/PhysRevLett.119.206401)

# Unconventional Chiral Fermions and Large Topological Fermi Arcs in RhSi

Guoqing Chang,<sup>1,2,\*</sup> Su-Yang Xu,<sup>3,\*</sup> Benjamin J. Wieder,<sup>4,\*</sup> Daniel S. Sanchez,<sup>3,\*</sup> Shin-Ming Huang,<sup>5</sup> Ilya Belopolski,<sup>3</sup> Tay-Rong Chang,<sup>6</sup> Songtian Zhang,<sup>3</sup> Arun Bansil,<sup>7</sup> Hsin Lin,<sup>1,2,†</sup> and M. Zahid Hasan<sup>3,†</sup>

<sup>1</sup>*Centre for Advanced 2D Materials and Graphene Research Centre  
National University of Singapore, 6 Science Drive 2, Singapore 117546*

<sup>2</sup>*Department of Physics, National University of Singapore, 2 Science Drive 3, Singapore 117542*

<sup>3</sup>*Laboratory for Topological Quantum Matter and Spectroscopy (B7),*

*Department of Physics, Princeton University, Princeton, New Jersey 08544, USA<sup>†</sup>*

<sup>4</sup>*Nordita, Center for Quantum Materials, KTH Royal Institute of Technology and Stockholm University,  
Roslagstullsbacken 23, SE-106 91 Stockholm, Sweden*

<sup>5</sup>*Department of Physics, National Sun Yat-Sen University, Kaohsiung 804, Taiwan*

<sup>6</sup>*Department of Physics, National Cheng Kung University, Tainan, 701, Taiwan*

<sup>7</sup>*Department of Physics, Northeastern University, Boston, Massachusetts 02115, USA*

The theoretical proposal of chiral fermions in topological semimetals has led to a significant effort towards their experimental realization. In particular, the Fermi surfaces of chiral semimetals carry quantized Chern numbers, making them an attractive platform for the observation of exotic transport and optical phenomena. While the simplest example of a chiral fermion in condensed matter is a conventional  $|C| = 1$  Weyl fermion, recent theoretical works have proposed a number of unconventional chiral fermions beyond the Standard Model which are protected by unique combinations of topology and crystalline symmetries. However, materials candidates for experimentally probing the transport and response signatures of these unconventional fermions have thus far remained elusive. In this paper, we propose the RhSi family in space group (SG) #198 as the ideal platform for the experimental examination of unconventional chiral fermions. We find that RhSi is a filling-enforced semimetal that features near its Fermi surface a chiral double six-fold-degenerate spin-1 Weyl node at  $R$  and a previously uncharacterized four-fold-degenerate chiral fermion at  $\Gamma$ . Each unconventional fermion displays Chern number  $\pm 4$  at the Fermi level. We also show that RhSi displays the largest possible momentum separation of compensative chiral fermions, the largest proposed topologically nontrivial energy window, and the longest possible Fermi arcs on its surface. We conclude by proposing signatures of an exotic bulk photogalvanic response in RhSi.

The allowed band crossings in condensed matter have, until recently, been considered closely linked to elementary particles in high-energy physics [1–4]. In 3D systems without spatial inversion ( $\mathcal{I}$ ) or time-reversal ( $\mathcal{T}$ ) symmetry, two-fold-degenerate band crossings are permitted, resulting in condensed matter realizations of Weyl fermions with quantized Chern numbers [1–24]. Since the experimental realization of the Weyl semimetal state in TaAs [18, 19], recent theoretical efforts have become focused on finding unconventional condensed matter quasi-particle excitations beyond the Dirac and Weyl paradigm described by the Standard Model [4, 28]. These efforts have rapidly expanded the set of known nodal features, which now additionally include symmorphic three-fold nexus fermions [25–27], eight-fold-degenerate double Dirac fermions [28], and, as detailed by Bradlyn, Cano, Wang, *et al.* (BCW) in Ref. 4, three-fold-degenerate single and six-fold-degenerate double spin-1 Weyl points. Unconventional chiral fermions, in particular, hold great promise for experimental applications, as they broaden beyond conventional Weyl semimetals the search for materials candidates for the observation of topological surface states, bulk chiral transport, and exotic circular photogalvanic effects [29–36].

Although the fundamental theory for these unconventional fermions has been established, one outstanding is-

sue has been the relative lack of ideal material candidates for their experimental examination. In the band structures of previously proposed materials, the unconventional fermions have typically sat away from the Fermi energy, or have in the cases of unconventional chiral fermions coexisted with additional, trivial bands. In these systems, while the unconventional fermions may be experimentally observable by photoemission, their topological properties are still prohibitively difficult to detect and utilize for transport and optical response. For example in MoP, a three-fold nexus fermion is observed 1 eV below the Fermi level, but the Fermi surface itself is unrelated to the three-fold fermion and carries no net Chern number [37].

In this paper, we identify the RhSi materials family of structurally chiral cubic crystals in space group (SG) 198  $P2_13$  [42] (Fig. 1(a)) as the first ideal materials candidates for the experimental study of the novel transport and response effects of unconventional chiral fermions. Using first-principles calculations detailed in Section A of the Supplemental Material (SM A), we find that the Fermi surface of RhSi consists of only two well-isolated pieces which carry equal and opposite quantized Chern number. The bulk bands near the Fermi energy feature a chiral six-fold-degenerate double spin-1 Weyl at the Brillouin zone (BZ) corner  $R$  and a previously uncharacter-

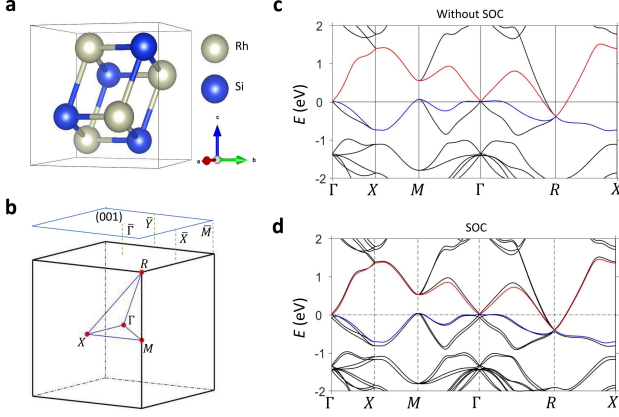


FIG. 1. **Lattice and electronic structure of RhSi in SG 198.** (a) Crystal structure of RhSi. Each unit cell contains 4 Rh and 4 Si atoms lying at Wyckoff positions with the minimum multiplicity of SG 198. (b) The cubic bulk Brillouin zone (BZ) of RhSi. (c) Band structure of RhSi in the absence of spin-orbit coupling (SOC). The highest valence and lowest conduction bands are colored in blue and red, respectively. (d) Band structure in the presence of SOC. A chiral double spin-1 Weyl point sits  $\sim 0.4\text{eV}$  below the Fermi energy at  $R$  and a previously uncharacterized four-fold-degenerate chiral fermion lies at the Fermi energy at  $\Gamma$ .

ized four-fold-degenerate chiral fermion at the zone center  $\Gamma$  (Fig. 1(c,d), Fig. 2(a,b)). RhSi therefore displays the *largest* possible separation of chiral fermions allowed in crystals. With an otherwise large bandgap, RhSi also therefore features the *largest* topologically nontrivial energy window proposed thus far (Fig. 1(d) and SM E). Furthermore, as these two chiral fermions lie at time-reversal-invariant momenta (TRIMs), they are unrelated by symmetry and free to exhibit an energy offset; here, the four-fold fermion at  $\Gamma$  lies roughly 400 meV above the six-fold fermion at  $R$ . This offset allows for the possibility of unique optical transport, such as the quantized circular photogalvanic effect [33]. Among all known chiral semimetals, both conventional Weyl and unconventional higher-fold fermion, RhSi therefore stands as possibly the most electronically ideal material yet proposed.

To understand the unusual high-fold-degenerate nodes displayed in the minimal band connectivity of SG 198, we construct an eight-band tight-binding (TB) model (SM C). SG 198 is characterized by three nonintersecting two-fold screw rotations  $s_{2x,y,z}$ , related by diagonal cubic three-fold rotation  $C_{3,111}$  [48]:

$$s_{2x} = \left\{ C_{2x} \begin{vmatrix} 1 & 1 \\ 2 & 2 \end{vmatrix} 0 \right\}, \quad s_{2y} = \left\{ C_{2y} \begin{vmatrix} 0 & 1 \\ 1 & 2 \end{vmatrix} \right\} \\ s_{2z} = \left\{ C_{2z} \begin{vmatrix} 1 & 0 \\ 2 & 2 \end{vmatrix} \right\}, \quad C_{3,111} = \left\{ C_{3,111} \begin{vmatrix} 0 & 0 & 0 \\ 0 & 0 & 0 \\ 0 & 0 & 0 \end{vmatrix} \right\}. \quad (1)$$

Without the three-fold rotation, this combination of screws and  $\mathcal{T}$ -symmetry characterizes orthorhombic SG

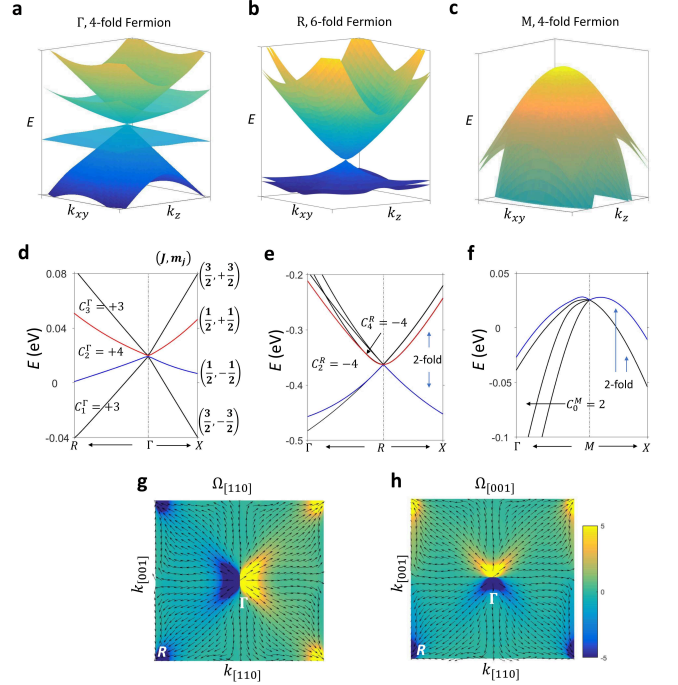


FIG. 2. **Energy dispersions and chiral character of the four-fold- and six-fold-degenerate unconventional fermions in RhSi.** (a,b,c) 3D energy dispersions of the degeneracies at  $\Gamma$ ,  $R$ , and  $M$ , respectively. (d,e,f) Band structures in the vicinities of  $\Gamma$ ,  $R$ , and  $M$ , respectively. Due to the local Kramers theorem enforced under the combined operation of  $(s_{2x,y,z} \times \mathcal{T})^2 = -1$ , bands along  $k_{x,y,z} = \pi$  are two-fold-degenerate (e,f). The absence of rotoinversion symmetries in SG 198 allows for nodes at TRIMs to have nontrivial Chern numbers; nodes with multiple finite- $q$  gaps can exhibit different Chern numbers occupying bands up to each gap (SM F) (d,e,f). At the Fermi energy, the four-fold-degenerate fermion at  $\Gamma$  has Chern number +4 and the double spin-1 Weyl at  $R$  has Chern number  $-4$ . The quadratic four-fold-degenerate crossing at  $M$  (f) also exhibits Chern number, but the bands dispersing from it are almost entirely covered by the Fermi energy. The four-fold-degenerate unconventional fermion at  $\Gamma$  (d) can be considered the combination of two  $J = 1/2$  and two  $J = 3/2$  states pinned together by time-reversal and screw symmetries. The analogous angular momentum eigenvalues for each band can then be deduced by observing the band eigenvalues of  $C_{3,111}$  and considering the symmetry-allowed term  $\vec{k} \cdot \vec{J}$  (SM C.2). (g,h) The Berry curvature  $\vec{\Omega}$  on the  $k_x = k_y$  plane flows almost directly from  $\Gamma$  to  $R$  with minimal out-of-plane deviations. Measuring the intensity of the  $xy$  (g) and  $z$  (h) components of  $\vec{\Omega}$ , we verify that  $\Gamma$  and  $R$  exhibit the local vector fields of  $C = \pm 4$  hedgehog defects.

19, and has been shown to force groups of eight or more bands to tangle together [39, 40, 49–51]. The additional cubic three-fold rotation  $C_{3,111}$  in SG 198 serves to increase the band degeneracy at TRIMs while still preserving this eight-band connectivity. At an electron filling of  $\nu \in 8\mathbb{Z} + 4$ , RhSi is gapless due to the com-

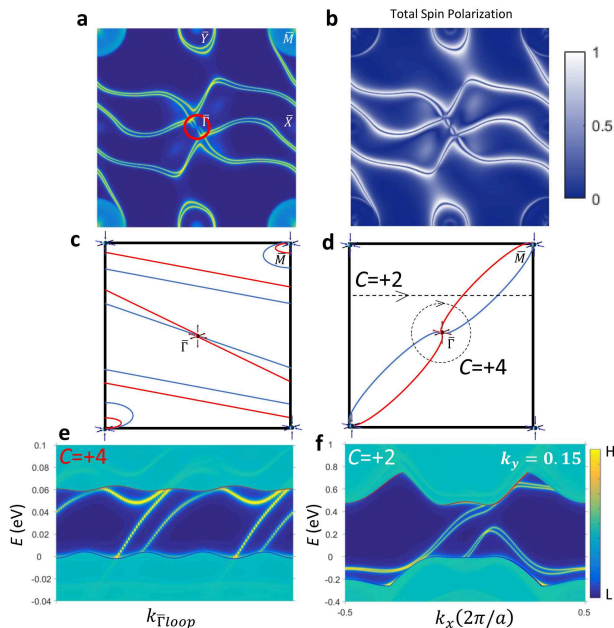


FIG. 3. **Surface state texture of RhSi** (a) The (001)-surface states of RhSi calculated using surface Green’s functions (SM A). Four Fermi arcs radiate at  $\bar{\Gamma}$  from the projection of the bulk four-fold-degenerate fermion at  $\Gamma$ , grouping into two time-reversed pairs and spiraling around the BZ (c) until they meet at  $\bar{M}$  at the projection of the bulk double spin-1 Weyl at  $R$ . (b) The surface states demonstrate  $\sim 80\%$  spin polarization (SM A). (d) An allowed simplified Fermi arc connectivity. For both possible connectivities (c,d), plotting the surface bands along a clockwise loop surrounding  $\bar{\Gamma}$  (red loop in (a), dashed loop in (d)), the surface bands (e) demonstrate a  $C = +4$  spectral flow. (f) Conversely, taking a loop along the zone-spanning dashed line at  $k_y = 0.15$  results in a surface state texture with just  $C = +2$  spectral flow, as only two Fermi arcs cross each half of the surface BZ.

bination of time-reversal and nonsymmorphic symmetries, and is therefore a “filling-enforced” semimetal (SM B) [39, 41, 49]. We find that our minimal TB model of SG 198 captures all of the degeneracy structure and topological character of RhSi. We list in SM C the irreducible corepresentations of the high-fold degeneracies at  $\Gamma$  and  $R$  in the language of Refs. 4, 28, and 48, and describe our results for the full BZ in detail; here we focus on characterizing the structure of the chiral nodes at  $\Gamma$  and  $R$ .

We begin by examining the band splitting and previously uncharacterized four-fold-degenerate unconventional chiral fermion at  $\Gamma$ . In the absence of SOC, our eight-band model permits only a single mass term at  $\Gamma$  which splits bands into a  $3 \times 2$ -fold-degenerate fermion and a doubly degenerate quadratic band, which in RhSi lies more than 2 eV above the Fermi energy (Fig. 1(c)). Upon the introduction of SOC, this quadratic crossing opens into a Kramers Weyl [24], and the  $3 \times 2$ -fold-degenerate node splits into a four-fold-degenerate

unconventional fermion and a second Kramers Weyl (Fig. 2(a,d)). This four-fold-degenerate fermion is distinct from the spin-3/2 chiral fermion introduced in Ref. 4: whereas that fermion is described by a corepresentation equivalent to the four-dimensional irreducible representation  $\bar{F}$  of chiral point group 432 ( $O$ ), the four-fold-degenerate fermion in RhSi is described by the  $\mathcal{T}$ -symmetric corepresentation formed by pairing the two-dimensional irreducible representations  ${}^1\bar{F}$  and  ${}^2\bar{F}$  of chiral point group 23 ( $T$ ) [48]. In the language of atomic orbitals, this four-fold degeneracy can be understood by modeling the six degenerate states without SOC by three  $p$  orbitals and an electron spin in the 111 direction. Calling  $z'$  the 111 direction and  $x', y'$  as orthonormal axes spanning the plane normal to  $z'$ , we group the  $p$  orbitals into a  $p_{z'}$ ,  $m_l = 0$  orbital and  $p_{x'} \pm ip_{y'}$ ,  $m_l = \pm 1$  orbitals. When coupled to the spin-1/2 electron, the six total states split into four  $J = 1/2$  and two  $J = 3/2$  states. Time-reversal pairs states with the same  $J$  and opposite  $m_j$ , and  $s_{2x}$  flips  $m_s$  without affecting  $m_l$ , such that under the SG 198 generators two  $J = 3/2$  states pair with two  $J = 1/2$  states and the remaining two  $J = 1/2$  states split off and form the second Kramers Weyl (SM C.2). By numerically calculating the eigenvalues of  $C_{3,111}$  and considering the symmetry-allowed term  $\vec{k} \cdot \vec{J}$ , each band near  $\Gamma$  can be assigned  $J$  and  $m_j$  eigenvalues, a structure we confirm explicitly with a symmetry-generated four-band  $k \cdot p$  model in SM C.2. As the irreducible representations at  $\Gamma$  are reflective of the position-space atomic orbitals [40], this analogy should also provide physical insight into the bonding character of RhSi. By integrating the Berry curvature between bands with  $J = 1/2$ ,  $m_j = \pm 1/2$  over a  $k$ -space sphere in the vicinity of  $\Gamma$  [3], we find that this unconventional fermion exhibits Chern number +4 at the Fermi level in RhSi (Fig. 2(d)).

Our examinations of the unconventional fermions at  $R$  with and without SOC (SM C.2) confirm the results of previous analyses of SGs 19 and 198 [4, 28, 49–51]. When SOC is taken into consideration, RhSi displays at  $R$  a six-fold-degenerate chiral double spin-1 Weyl at  $\sim 0.4\text{eV}$  below the Fermi level, which at the finite- $q$  gap spanned by the Fermi energy exhibits Chern number  $-4$  (Fig. 2(b,e)). Projecting out of our TB model the six-band subspace of this chiral fermion results in a  $k \cdot p$  theory related by a unitary transformation to that presented in Ref. 4 of two coupled spin-1 fermions with individual  $\vec{k} \cdot \vec{S}$  dispersion.

Calculating the surface states of RhSi (Fig. 3(a)) through surface Green’s functions (SM A), we find that the (001)-surface displays four topological Fermi arcs connecting the projections of the bulk chiral fermions at  $\bar{\Gamma}$  to those at  $\bar{M}$  across the entire surface BZ. Unlike the recently observed trivial arcs in  $\text{WTe}_2$  [23, 52], the long Fermi arcs in RhSi are guaranteed by bulk topology, and should therefore be robust against changes in surface chemical potential and disorder (SM E). Though the arcs

in our calculations demonstrate a particularly elaborate connectivity (Fig. 3(c)), a much simpler direct connectivity is also allowed (Fig. 3(d)). We also find the Fermi arcs to have  $\sim 80\%$  spin polarization [53] (Fig. 3(b)). Therefore, RhSi is also an attractive platform for spintronic applications [54, 55].

To summarize our analysis of the electronic structure of RhSi, we find that it is a remarkably ideal candidate for the observation of chiral transport and optical phenomena and for the direct examination of unconventional fermions. Bands within the  $k \cdot p$  regime of the unconventional fermions at  $\Gamma$  and  $R$  cleanly characterize the *entire* Fermi surface, such that the separation between Fermi pockets of opposite Chern number is the *entire length* of the 3D diagonal of the BZ cube. The remaining bulk band manifolds are otherwise separated by a gap of  $\sim 1.2$  eV (Fig. 1(d)), such that RhSi has *by far* the largest topologically nontrivial energy window of any previously proposed or experimentally realized chiral semimetal (SM E). RhSi also therefore displays on its surface topologically-guaranteed Fermi arcs that span *the entire* surface BZ, and uniquely come in time-reversed pairs (Fig. 3). Finally, unlike in previous band-inversion Weyl semimetals where pairs of Weyl points have been related by mirror symmetry, the chiral fermions in RhSi are free to sit with an energy offset, enabling chiral photogalvanic transport [33].

We therefore conclude with a numerical prediction of quantized optical transport in RhSi. In Ref. 33, the authors show that in a structurally chiral system for which only a single two-band Weyl fermion is partially unoccupied, such as a Kramers Weyl metal [24], the difference in the rate of current density resulting from exciting electrons with left- and right-handed circularly polarized light is quantized in terms of fundamental constants:

$$\frac{dj}{dt} = \frac{2I\beta_0}{c\epsilon_0}C, \quad \beta_0 = \frac{\pi e^3}{h^2}, \quad (2)$$

where  $I$  is the intensity of applied light and  $C$  is the Chern number of the Weyl point (Fig. 4(a,b)). In RhSi, the four-fold fermion at  $\Gamma$  sits just above the Fermi energy while the chiral double spin-1 Weyl at  $R$  sits below and is fully occupied; the location of the chiral fermions in its band structure (Fig. 1(d)) is *practically identical* to the ideal case proposed in Ref. 33. We observe that the angular momentum selection rules for circularly polarized light appear to strongly constrain the allowed transitions in this four-fold fermion, such that only transitions between bands with  $\Delta m_j = \pm 1$  contribute to the photocurrent [56]. Therefore, when weighting by Fermi occupation factors, the photocurrent rate calculated from the trace of the gyrotropic tensor (SM D), though initially fluctuating, still saturates at the quantized value  $(2I\beta_0/c\epsilon_0) \times 4$  with increasing incident photon energy  $E_p$  in the vicinity of  $\Gamma$ , or four times the value predicted for a conventional Weyl fermion (Fig. 4(b,d)). Therefore, despite the multi-

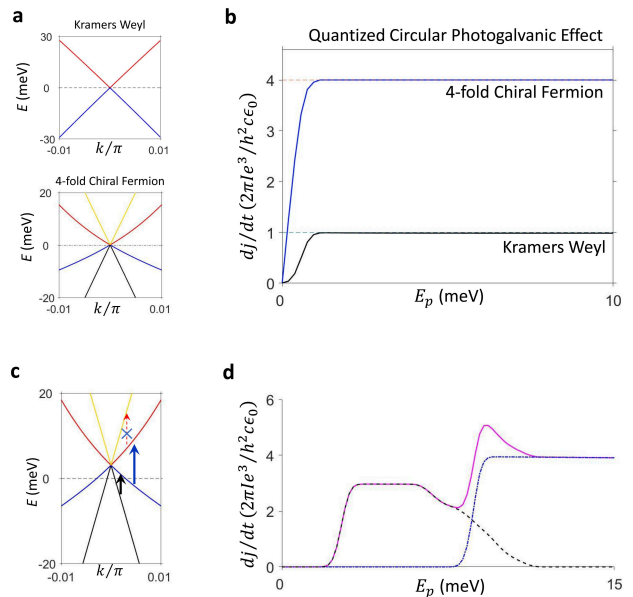


FIG. 4. **Quantized circular photogalvanic effect (CPGE) of the four-fold-degenerate unconventional fermion in RhSi** (a,b) The CPGE of a single conventional Weyl node as proposed in Ref. [33]. (b) Calculations of the CPGE for the four-fold unconventional fermion at  $\Gamma$  in RhSi, tuned to half-filling. The photocurrent rate saturates at four times the value it did for the conventional Weyl in (a), as the Chern number in this gap is four times as large. (c) The more realistic case of a partial occupation of this four-fold fermion; multiple transitions contribute to the photocurrent. (d) Contributions to the traced photocurrent rate from each transition in (c), calculated from the fitted TB model (SM C.3). Trend lines in (d) are labeled by the color of their contributing transition in (c), with pink representing the overall photocurrent rate.

band complexities of its unconventional chiral fermions, RhSi remains a plausible candidate for probing the quantized photogalvanic effect.

The authors thank Charles L. Kane, Barry Bradlyn, Jennifer Cano, and B. A. Bernevig for invaluable discussions. BJW was supported through Nordita under ERC DM 321031.

\* These authors contributed equally to this work.

† Corresponding authors (emails):  
 suyangxu@princeton.edu, nilnish@gmail.com,  
 mzhasan@princeton.edu

- [1] H. Weyl, *Z. Phys.* **56**, 330-352 (1929).
- [2] F. Wilczek, *Phys. Today* **51**, 11-13 (1998).
- [3] G. E. Volovik, *The Universe in a Helium Droplet* (Clarendon Press, Oxford, 2003).
- [4] B. Bradlyn *et al.*, *Science* **353**, 6299 (2016).
- [5] C. L. Kane and E. J. Mele, *Phys. Rev. Lett.* **95**, 226801 (2005).

- [6] C. L. Kane and E. J. Mele, Phys. Rev. Lett. **95**, 146802 (2005).
- [7] M. Z. Hasan and C. L. Kane, Rev. Mod. Phys. **82**, 3045 (2010).
- [8] X.-L. Qi and S.-C. Zhang, Rev. Mod. Phys. **83**, 1057 (2011).
- [9] B. A. Bernevig, T. L. Hughes, and S.-C. Zhang, Science **314**, 1757 (2006).
- [10] A. Bansil, H. Lin, and T. Das, Rev. Mod. Phys. **88**, 021004 (2016).
- [11] M. Z. Hasan, S.-Y. Xu, I. Belopolski, and S.-M. Huang, Annual Review of Condensed Matter Physics **8** 289-309 (2017).
- [12] N. P. Armitage, E. J. Mele, A. Vishwanath, Preprint at <https://arxiv.org/abs/1705.01111> (2017).
- [13] X. Wan *et al.*, Phys. Rev. B **83**, 205101 (2011).
- [14] A. A. Burkov and L. Balents, Phys. Rev. Lett. **107**, 127205 (2011).
- [15] S. Murakami, New Journal of Physics **9**, 356 (2007).
- [16] S.-M. Huang, S.-Y. Xu *et al.*, Nature Communications **6**, 7373 (2015).
- [17] H. Weng *et al.*, Phys. Rev. X **5**, 011029 (2015).
- [18] S.-Y. Xu *et al.*, Science **349**, 613 (2015).
- [19] B. Q. Lv *et al.*, Phys. Rev. X **5**, 031013 (2015).
- [20] L. Lu *et al.*, Science **349**, 622 (2015).
- [21] A. A. Soluyanov *et al.*, Nature **527**, 495 (2015).
- [22] Y. Xu, F. Zhang and C. Zhang, Phys. Rev. Lett. **115**, 265305 (2015).
- [23] S.-Y. Xu *et al.*, Science Advances, **3**(6), e1603266 (2017).
- [24] G. Chang *et al.*, Preprint at <https://arxiv.org/abs/1611.07925> (2016).
- [25] H. Weng, C. Fang, Z. Fang, and X. Dai, Phys. Rev. B **93**, 241202 (2016).
- [26] Z. Zhu, G. W. Winkler, Q. Wu, J. Li, and A. A. Soluyanov, Phys. Rev. X **6**, 031003 (2016).
- [27] G. Chang *et al.*, Scientific Reports **7**, 1688 (2017).
- [28] B. J. Wieder, Y. Kim, A. M. Rappe, and C. L. Kane, Phys. Rev. Lett. **116**, 186402 (2016).
- [29] S. Zhong, J. E. Moore, and I. Souza, Phys. Rev. Lett. **116**, 077201 (2016).
- [30] J. Ma and D. A. Pesin, Phys. Rev. B **92**, 235205 (2015).
- [31] C.-K. Chan *et al.*, Phys. Rev. B **95**, 041104 (R) (2017).
- [32] Q. Ma, S.-Y. Xu *et al.*, Nature physics doi:10.1038/nphys4146 (2017).
- [33] F. de Juan *et al.*, Nature Communications **8**, 15995 (2017).
- [34] L. Balents, Physics **4**, 36 (2011).
- [35] T. Ojanen, Phys. Rev. B **87**, 245112 (2013).
- [36] C. Fang, L. Lu, J. Liu, and L. Fu, Nat. Phys. **12**, 936 (2016).
- [37] B. Q. Lv *et al.*, Nature **546**, 627 (2017).
- [38] P. Demchenko *et al.*, Chem. Met. Alloys **1**, 50 (2008).
- [39] H. Watanabe, H. C. Po, A. Vishwanath, and M. Zaletel, PNAS **112**, 14551 (2015).
- [40] B. Bradlyn *et al.*, Nature **547**, 298 (2017).
- [41] S. M. Young and B. J. Wieder, Phys. Rev. Lett. **118**, 186401 (2017).
- [42] I. Engström and J. Torsten, Acta Chemica Scandinavica **19**, 1508 (1965).
- [43] G. Wenski and A. Mewis, Zeitschrift für anorganische und allgemeine Chemie **535**, 110 (1986).
- [44] H. Takizawa, T. Sato, T. Endo, and M. Shimada, Journal of Solid State Chemistry **73**, 40 (1988).
- [45] V. Larchev and S. Popova, Journal of the Less Common Metals **87**, 53 (1982).
- [46] M. Etnenberg, K. L. Komarek, and E. Miller, Metallurgical Transactions **2**, 1173 (1971).
- [47] K. Schubert *et al.*, Naturwissenschaften **43**, 248 (1956).
- [48] C. J. Bradley and A. P. Cracknell, The Mathematical Theory of Symmetry in Solids (Clarendon Press Oxford, Oxford, United Kingdom, 1972), ISBN 0199582580.
- [49] B. J. Wieder and C. L. Kane, Phys. Rev. B **94**, 155108 (2016).
- [50] A. Bouhon and A. Black-Schaffer, Phys. Rev. B **95**, 241101(R) (2017).
- [51] R. M. Geilhufe, S. S. Borysov, A. Bouhon, and A. V. Balatsky, Preprint at <https://arxiv.org/abs/1611.04316> (2017).
- [52] F.Y. Bruno *et al.*, Phys. Rev. B **94**, 121112(R) (2016).
- [53] S.-Y. Xu *et al.*, Phys. Rev. Lett. **116**, 096801 (2016).
- [54] I. Žutić, J. Fabian, and S. Das Sarma, Rev. Mod. Phys. **76**, 323 (2004).
- [55] A. R. Mellnik *et al.*, Nature **511**, 449 (2014).
- [56] C. L. Tang and H. Rabin, Phys. Rev. B **3**, 4025 (1971).